Electronic Supplementary Information DOI: 10.1039/C5EE02870A

Molecular-Ink Route to 13.0% Efficient Low-Bandgap $CuIn(S,Se)_2$ and 14.7% Efficient $Cu(In,Ga)(S,Se)_2$ Solar Cells

A. R. Uhl,*[a] J. K. Katahara[a] and H. W. Hillhouse*[a]

[a] Department of Chemical Engineering, Molecular Engineering and Sciences, Institute, University of Washington, Box 351750, Seattle, WA 98195-1750, USA. Email: auhl@uw.edu; h2@uw.edu.

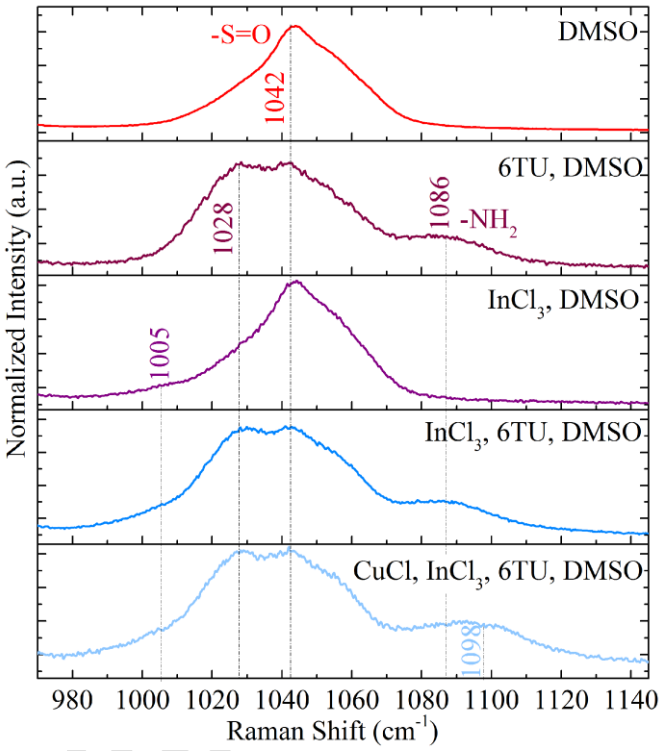

Fig. S1. The DMSO S=O stretching vibration at 1042 cm^{-1} moves to lower wavenumbers with addition of $InCl_3$, supporting the coordination of $InCl_3$ with DMSO through oxygen. The coordination stays intact regardless of the addition of thiourea and CuCl.

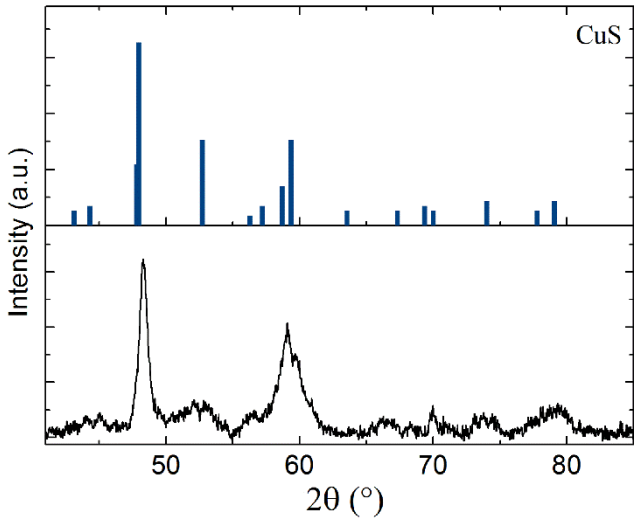

Fig. S2. Powder X-ray diffraction pattern of precipitated crystals from an ink with TU/Me ratio of 0.5 (Figure 2b) indicates the formation of Cu(II)S crystals. EDX measurements corroborate that finding (Cu/S (at%/at%) = 0.99).

Table S1. ICP-MS compositional study (in at.%) at varying thiourea to metal ratios (TU/Me) for unfiltered inks.

		Cu/In	In loss (%)
TU/Me=3	ink	0.92	-2 ± 2
	precursor	0.91	
	absorber	0.89	
TU/Me=2	ink	0.95	-2 ± 2
	precursor	0.92	
	absorber	0.93	
TU/Me=1	ink	0.91	2 ± 2
	precursor	0.92	
	absorber	0.93	

Table S2. PV parameters of $CuIn(S,Se)_2$ (CIS) and $Cu(In,Ga)(S,Se)_2$ (CIGS) record cells as presented in Figure 3d.

	PCE (%)	FF (%)	Voc (mV)	Jsc (mA cm^{-2})	Avg. PCE* (%)	Rs (Ω cm^2)	Rsh (Ω cm^2)	A	Jo (mA cm^{-2})	Egap (eV)	τ (ns)
CIS	13.0	68.3	507	37.4	12.8 ± 0.4	0.8	743	1.59	1.6×10^{-4}	1.00	5.0
CIGS	14.7	71.5	661	31.2	13.3 ± 0.5	1.4	856	1.48	8.2×10^{-7}	1.15	21

*calculated from the ten best cells on two substrates.

Table S3. Single crystal X-ray diffraction crystallographic data for the $In(DMSO)_3Cl_3$ structure in Figure 1b. Cif files have been deposited with the Cambridge Crystallographic Data Centre (CCDC) under the number 1423406.

Empirical formula	C6 H18 Cl3 In O3 S3	
Formula weight	455.55	
Temperature	90(2) K	
Wavelength	0.71073 Å	
Crystal system	Triclinic	
Space group	P - 1	
Unit cell dimensions	a = 7.7728(4) Å	α= 81.826(4)°
	b = 8.7954(6) Å	β= 79.433(3)°
	c = 13.4794(7) Å	γ = 64.156(2)°
Volume	813.27(8) Å^3	
Z	2	
Density (calculated)	1.860 Mg/m^3	
Absorption coefficient	2.321 mm^{-1}	
F(000)	452	
Crystal size	0.20 x 0.15 x 0.10 mm^3	
Theta range for data collection	2.58 to 30.73°	
Index ranges	-11<=h<=10, -12<=k<=12, -19<=l<=0	
Reflections collected	4912	
Independent reflections	4912 [R(int) = 0.0348]	
Completeness to theta = 25.00°	99.5 %	
Max. and min. transmission	0.8011 and 0.6539	
Refinement method	Full-matrix least-squares on F^2	
Data / restraints / parameters	4912 / 0 / 151	
Goodness-of-fit on F^2	1.070	
Final R indices [I>2sigma(I)]	R1 = 0.0348, wR2 = 0.0684	
R indices (all data)	R1 = 0.0461, wR2 = 0.0715	
Largest diff. peak and hole	0.826 and -1.244 e.Å^{-3}	

Table S4. Chemical reactions that show the coordination of copper and indium complexes as determined by single crystal XRD, powder XRD, Raman, and the visual appearance of the inks. The data and previous reports suggest that an additional TU coordinates to copper in solution (as compared to the crystal).

Indium-free Ink

$$CuCl_{(s)} + 6\ TU_{(s)} + x\ DMSO_{(l)} \rightarrow Cu(TU)_3Cl_{(s)} + 3\ TU_{(s)} + x\ DMSO_{(g)} \quad (1a)$$

$$CuCl_{(s)} + 6\ TU_{(s)} + x\ DMSO_{(l)} \rightarrow Cu(TU)_4Cl_{(solv)} + 2\ TU_{(solv)} + x\ DMSO_{(l)} \quad (1b)$$

Copper-free Ink

$$InCl_{3(s)} + 6\ TU_{(s)} + x\ DMSO_{(l)} \rightarrow In(DMSO)_3Cl_{3(solv)} + 6\ TU_{(solv)} + (x-3)\ DMSO_{(l)} \quad (2)$$

Combined Final Ink

$$CuCl_{(s)} + InCl_{3(s)} + 6\ TU_{(s)} + x\ DMSO_{(l)} \rightarrow$$

$$\rightarrow In(DMSO)_3Cl_{3(solv)} + Cu(TU)_4Cl_{(solv)} + 2\ TU_{(solv)} + (x-3)\ DMSO_{(l)} \quad (3)$$

Ink and device preparation

Ink preparation: The ink preparation, deposition, and annealing was carried out in a N_2 filled glove box with controlled O_2 and H_2O content below 20 ppm. To prepare the precursor solutions, 2.5 M TU (recrystallized, 99%, Aldrich), 0.38 M CuCl (99.995%, Aldrich), and 0.45 M $InCl_3$ (99.999%, Aldrich) were added to DMSO (99.9%, Aldrich). The reagents were added consecutively to the ink and allowed to dissolve under stirring before adding the next. After the addition of $InCl_3$, the inks were heated for 2 h at 120°C to form a clear solution. For the gallium containing inks in Figure 3, 0.14 M $GaCl_3$ (99.99%, Aldrich) was additionally added after dissolving 3.0 M thiourea, 0.40 M CuCl, and 0.33 M $InCl_3$ in DMSO.

Solar cell processing: For the precursor samples, inks were filtered with 0.45 µm PTFE filters, spin-coated at 1300 rpm for 1 min on molybdenum-coated soda lime glass substrates, and annealed on a hotplate at 250°C for 2 min. For the cells in Figure 3, 13 coating and annealing cycles were used to build the desired layer thickness. The samples were then placed in a graphite box with selenium pellets (99.99%, Aldrich) and annealed at 540°C for 20 min under flowing Ar (99.998%) and pressures close to atmosphere (1000 torr) to convert precursor films to absorber layers. KCN etching (97%, Fluka) of the absorbers for 1 min in 10 wt.% aqueous solution was carried out for the Ga-containing sample only. A 30 nm thick CdS layer was deposited on the substrates by chemical bath deposition from an aqueous solution of 1.5 mM CdSO4 (99.996%, Alfa Aesar), 1.9 M NH4OH (ACS grade, EMS), and 74 mM TU (recrystallized, 99%, Aldrich) for 12 min at 65°C. The solar cells were finished with 50 nm of i-ZnO and 250 nm ITO layer by RF-sputtering, Ni/Al grid contacts by thermal evaporation (50/1000 nm), and a 110 nm thick MgF_2 layer by e-beam evaporation. The solar cell area was defined by manual scribing to a cell area of 0.11 and 0.42 cm^2.

Characterization of inks and layers

Solar cell performance measurements: Current-voltage (I-V) and EQE measurements were carried out under simulated standard testing conditions according to ASTM E948-09 (25°C, 1000 W/m^2, AM1.5G illumination). The measurement error of device parameters is estimated to be less than 3%.

X-ray diffraction: For the single crystal X-ray diffraction (Figure 1b), the precursor ink was slowly cooled in a water bath from 120°C to room temperature until small crystallites precipitated. A colorless prism, measuring 0.20 x 0.15 x 0.10 mm^3 was mounted on a loop with oil. Data was collected at -183°C on a Bruker APEX II single crystal X-ray diffractometer with Mo-radiation at 0.71073 Å. The crystal-to-detector distance was 40 mm and the exposure time was 10 seconds per frame for all sets. The scan width was 0.5°. The crystal appeared with triclinic lattice structure with the empirical formula C6 H18 Cl3 In O3 S3 and unit cell dimensions a = 7.7728(4) Å, b = 8.7954(6) Å, c = 13.4794(7) Å, α = 81.826(4)°, β= 79.433(3)°, and γ = 64.156(2)° (see Table S3). Powder X-ray diffraction measurements (Figure 1d, 3a, S2) were carried out on a Bruker D8 Discover with GADDS (General Area Detector Diffraction System), equipped with automated Laser-Video alignment system, rotating Cu anode (λ = 1.542 Å) and Hi-Star 2D detector. The instrument was operated in parallel-beam geometry with a 0.5 mm beam diameter and instrument related peak broadening of 0.3° in 2 θ. All samples were scanned at 40 kV and 120 mA with a step size of 0.02°. Reference patterns were retrieved from ICSD and ICDD database ($Cu(TU)_3Cl_3$: 01-072-1097, TU: 01-076-1127, $CuInSe_2$: 40-1487, $MoSe_2$: 29-914, CuS: 00-006-0464). To obtain crystals in Figure 1d, an $InCl_3$-free precursor ink was heated at 100°C in N_2 atmosphere and reduced pressure (1 torr) until the solvent evaporated and solid crystals precipitated. Crystals in Figure S2 were obtained by decantation of a precursor ink with TU/Cu = 0.5. Materials Studio 7.0 with the Dmol3 package was used for the 3D graphical representation of the crystal structures.

Thermogravimetric analysis and Fourier transform infrared spectroscopy: Decomposition studies of the ink were carried out on a TA Instruments TGA Q50, equipped with an EGA furnace, and Bruker Vertex 70 FTIR. The liquid sample was heated in an alumina cup at a rate of 5°C/min under continuous N_2 flow (balance: 10 ml/min, sample: 90 ml/min). FTIR was measured from 4000 cm^{-1} to 600 cm^{-1} with a resolution of 2 cm^{-1}. During the TGA run, FTIR spectra were recorded every 30 seconds and consisted of 36 averaged individual scans. CO_2 and H_2O compensation was applied to the data with OPUS v7.2. DMSO and CS_2 absorptions in Figure 1e were matched to reference data from the EPA-NIST vapor phase library (DMSO: 3608, CS_2: 3234).

Raman spectroscopy: All Raman spectra were collected on a LabRAM HR-800 (HORIBA-Jobin Yvon). A 532 nm diode-pumped solid-state laser (Nd:YAG) was focused through a 10x Olympus MPlan achromatic dry objective into a quartz cuvette (1 cm path length) containing the inks. The scattered light was spectrally resolved through an 1800 l/mm Czerny-Turner monochromator (blazed at 750nm) and passed to a Peltier-cooled Si charge coupled device (CCD) detector. The microscope objective was focused to maximize the DMSO C-S symmetric stretch at 670 cm^{-1} (typically 3 mm below the cuvette top surface). The excitation intensity was roughly 7 mW, and the collection time was 1 s with 5 replicates averaged to reduce noise.

Inductively coupled plasma mass spectroscopy: Elemental concentrations of Cu, In, S, and Se were determined by ICP-MS using a Perkin Elmer DRC-e. Solid samples, i.e. precursor and absorber layers, were scratched off from the substrate with borosilicate pipettes and digested at 80°C for 12h in 18 MΩ Milli-Q H_2O with 2.0 vol.% H_2O_2 (TraceSELECT grade, Fluka), 0.5 vol.% HCl (99.999%, Aldrich), and 1.5 vol.% HNO_3 (99.999%, Aldrich) solutions. All elements were calibrated from 2 µg/l to 20 mg/l by matrix matched dilutions from stock solutions (1000 mg/l, Fluka Analytical). The measurements were carried out in dynamic reaction cell mode (DRC) with NH_3 and O_2 gases to allow for unambiguous quantification.

Scanning electron microscopy: The scanning electron micrograph was conducted on a FEI Sirion XL-30 with field emission gun and an Oxford energy dispersive X-ray spectrometry (EDS) detector. Secondary electrons were used for imaging and compositional measurements at 5 kV and 20 kV acceleration voltage, respectively, and a working distance of 5 mm. The cross-section of a cleaved sample was coated with carbon to reduce charging.

Time-resolved photoluminescence: The minority carrier lifetimes in Table S2 were measured on the finished devices with a PicoQuant FluoTime 300 with a Hamamatsu infrared sensitive photomultiplier tube, 780 nm excitation, and 808 nm long-pass filter on the emission side. The intensity weighted average lifetimes were determined after reconvolution with the system response and bi-exponential fit of the decays.